ACS APPLIED MATERIALS & INTERFACES

www.acsami.org

Forum Article

Reagent-Free Lactate Detection Using Prussian Blue and Electropolymerized-Molecularly Imprinted Polymers-Based Electrochemical Biosensors

Grace Dykstra, Isabel Chapa, and Yixin Liu*

Cite This: ACS Appl. Mater. Interfaces 2024, 16, 66921−66931

Read Online

ACCESS | Metrics & More | Article Recommendations | Supporting Information

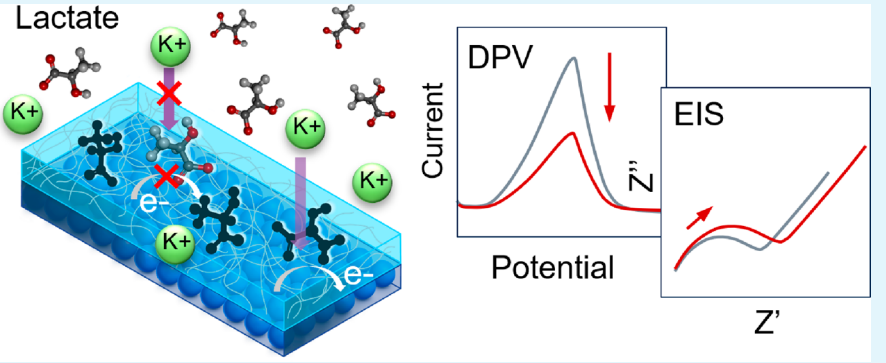

ABSTRACT: Sweat lactate, a promising biomarker for assessing physical performance and health conditions, calls for noninvasive, convenient, and affordable detection methods. This study leverages molecularly imprinted polymers (MIPs) as a synthetic biorecognition element for lactate detection due to their affordability and high stability. Traditional MIPs-based electrochemical sensors often require external redox probes such as ferricyanide/ferrocyanide in the solution to signal the binding between analytes and MIPs, which restricts their applicability. To address this, our study introduces an innovative approach utilizing a layer of Prussian blue (PB) nanoparticles as the internal redox probe on screen-printed carbon electrodes (SPCE), followed by a layer of electropolymerized MIP (eMIP) for molecular recognition, enabling reagent-free lactate detection. The real-time growth of eMIP and the processes of template elution and lactate rebinding were examined and validated using electrochemical surface plasmon resonance (EC-SPR) spectroscopy. The sensor's performance was thoroughly investigated using Differential Pulsed Voltammetry (DPV) and Electrochemical Impedance Spectroscopy (EIS) with samples spiked in 0.1 M KCl solution and artificial sweat. The developed sensors demonstrated a fast and selective response to lactate, detecting concentrations from 1 to 35 mM with a Limit of Detection (LOD) of 0.20 mM, defined by a signal-to-noise ratio of 3 in the DPV measurements. They also exhibited excellent reproducibility, reusability, and a shelf life of up to 10 months under ambient conditions. These eMIP/PB/SPCE-based lactate sensors show considerable potential as point-of-care (POC) devices for sweat lactate detection, and the technology could be adapted for reagent-free detection of a broad spectrum of molecules.

KEYWORDS: *molecularly imprinted polymer, Prussian blue, lactate detection, electrochemical biosensor, reagent-free detection*

1. INTRODUCTION

Sweat lactate, an excellent biomarker of tissue oxygenation, provides valuable insights into energy metabolism,[1] making it a promising candidate for assessing physical performance in sports, military, and healthcare applications. Its production increases with exercise intensity,[2,3] which can reach up to 25 mM during intense exercise.[4] A surge in lactate production can lead to cell acidosis and a disruption in muscle performance. It can also indicate pressure ischemia and serve as a progression biomarker for tissue perfusion.[5] Therefore, detecting sweat lactate offers a noninvasive and convenient approach for evaluating exercise intensity, optimizing athletic training and performance, and facilitating medical diagnosis and monitoring.

The rapid advancement of biosensing, microfluidics, flexible electronics, and wireless communications technologies has led to the development of wearable biosensors for sweat analysis,[6−10] including lactate monitoring.[11−13] However,

Special Issue: Early Career Forum 2024

Received: December 27, 2023
Revised: April 13, 2024
Accepted: April 19, 2024
Published: May 1, 2024

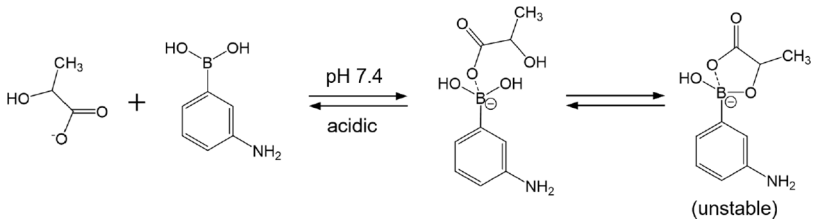

these lactate sensors predominantly incorporate enzymes such as lactate oxidase and lactate dehydrogenase,[14,15] which often face stability issues due to temperature and pH variations.[16] As an alternative, Molecularly Imprinted Polymers (MIPs) have emerged as tailored synthetic molecular recognition elements, offering remarkable cost-effectiveness and superior stability. MIPs are synthesized through the self-assembly and polymerization of functional monomers around template molecules, i.e., the analyte. This process results in the formation of molecular recognition cavities within a polymer matrix once the template molecules are removed. They have been integrated with different transducing mechanisms (e.g., electrochemical, fluorescent, optical, etc.)[17−20] for a wide range of analyte detection, including small molecules, proteins, and pathogens.[21]

In the realm of wearable biosensors, electrochemical sensors provide remarkable advantages such as low cost, rapid detection, high selectivity and sensitivity, and ease of miniaturization.[9,22] Electropolymerization offers a fast and facile one-step approach to constructing MIP-based electrochemical sensors, which directly deposits a MIP layer onto the electrode surface,[23−25] significantly simplifying the fabrication process. However, most MIP-based electrochemical sensors require external redox couples (e.g., ferricyanide/ferrocyanide) to signal the binding events between electrochemically inactive analytes and the MIP. This could disrupt the interaction between the MIP and analyte molecules and pose challenges for on-body operation. Therefore, there is a pressing need to develop reagent-free MIP-based biosensors for simple and convenient lactate detection and the advancement of wearable MIP-based biosensors.

Prussian Blue (PB) is one of the most representative electron-transfer mediators for enzymatic biosensors.[26−28] It comprises iron atoms in Fe(II) and Fe(III) oxidation states, bridged by cyanide groups in a cubic crystal structure with the formula $Fe_4^{III}[Fe^{II}(CN)_6]_3$. PB shows excellent redox activity with electron transfer compensated by the entrapment and release of cations (i.e., K^+),[29] making it an attractive internal redox probe for MIP signaling. It has been reported that PB can be coelectrodeposited with MIP to form a PB-embedded MIP for self-signaling.[30] However, PB electrodeposition typically requires a highly acidic solution, which is not ideal for the imprinting processes where functional monomers and template molecules bind at higher pH. For example, 3-aminophenylboronic acid (3-APBA) is a functional monomer that interacts with lactate in neutral or alkaline pH, as shown below. Such interaction dissociates in an acidic environment,[31,32] making PB-MIP codeposition unsuitable for lactate imprinting.

In this study, we introduce a regent-free, nonenzymatic lactate sensor, entirely constructed using electrochemical techniques. The sensor features a layer of electrodeposited PB as the internal redox probe and a layer of electropolymerized MIP (eMIP), employing 3-APBA and pyrrole as functional monomers for the selective recognition of lactate. The sequential layering of PB and eMIP allows for successful PB deposition in an acidic environment and eMIP polymerization in a neutral environment, facilitating the formation of the 3-APBA-lactate recognition complex. The eMIP growth, template removal, and lactate rebinding processes were investigated and validated in real time using Electrochemical-Surface Plasmon Resonance (EC-SPR). The performance of the sensor was evaluated in both spiked 0.1 M KCl solution and artificial sweat (AS) using Differential Pulse Voltammetry (DPV) and Electrochemical Impedance Spectroscopy (EIS). The lactate sensor demonstrated excellent sensitivity and repeatability throughout repeated testing and maintained a long shelf life of 10 months. The lactate sensor developed holds great potential for direct-sweat lactate analysis, and the design and fabrication process of this sensor could be tailored to create a broad range of eMIP-based electrochemical sensors for the detection of various other molecules.

2. MATERIALS AND EXPERIMENTAL DETAILS

2.1. Reagents and Instruments. Iron(III) chloride hexahydrate ($FeCl_3$), potassium hexacyanoferrate(III), potassium hexacyanoferrate(II) trihydrate, potassium chloride (KCl), phosphate-buffered saline (PBS) tablets (pH 7.4), sodium lactate, uric acid, acetaminophen, ascorbic acid, urea, glucose, acetic acid, lactic acid, sulfuric acid, potassium hydroxide (KOH), and 3-aminophenylboronic acid (3-APBA) were purchased from Sigma-Aldrich (St. Louis, MO, USA). Hydrogen chloride (HCl) and sulfuric acid (98%) were purchased from Fisher Chemicals (St. Louis, MO, USA). Pyrrole (99%) was purchased from Acros Organics (Fair Lawn, NJ, USA). Screen-Printed Carbon Electrodes (SPCE) featuring a carbon working electrode (3 mm diameter), a carbon counter electrode, and a Ag/AgCl reference electrode were purchased from Zensor (Taiwan). The DI water was produced using the Sartorius arium mini DI water purification system (Göttingen, Germany). Electrochemical measurements were taken using a PalmSens MultiEMStat3 (a 12-channel potentiostat) and PalmSens4 (GA Houten, Netherlands). EC-SPR study was performed on gold chips using nanoSPR-77, purchased from Nano SPR (Chicago, IL, USA). A Hitachi S-4700 Field Emission Scanning Electron Microscope (FE-SEM) was used to acquire the SEM images.

2.2. Preparation of Screen-Printed Carbon Electrodes. Each SPCE initially underwent a cleaning and activation process via cyclic voltammetry (CV) in 80 μL of 0.5 M sulfuric acid, cycling within a potential range of −1.5 to 1.5 V at a scan rate of 100 mV s^{-1} for 20 cycles. This step acts to remove any potential residue on the SPCE from the manufacturing process while simultaneously activating the electrode's surface. Following this, the electrode was thoroughly rinsed and allowed to air-dry prior to use.

2.3. Deposition of Prussian Blue on SPCE. Prussian blue nanoparticles were electrodeposited onto the SPCE surface by using an 80 μL solution containing 3 mM $FeCl_3$, 3 mM $K_3Fe^{III}(CN)_6$, 0.1 M KCl, and 0.1 M HCl. This deposition process was achieved through cyclic voltammetry within a potential range of −0.2 to 0.6 V for 20 cycles at a scan rate of 50 mV s^{-1}. Following deposition, the electrode, denoted as PB/SPCE, was carefully rinsed with water and then left to dry.

2.4. Synthesis of Lactate eMIP Layer on PB/SPCE. Following PB deposition, an eMIP layer was fabricated on top of the PB nanoparticles using electropolymerization with an 80 μL solution

https://doi.org/10.1021/acsami.3c19448
ACS Appl. Mater. Interfaces 2024, 16, 66921−66931

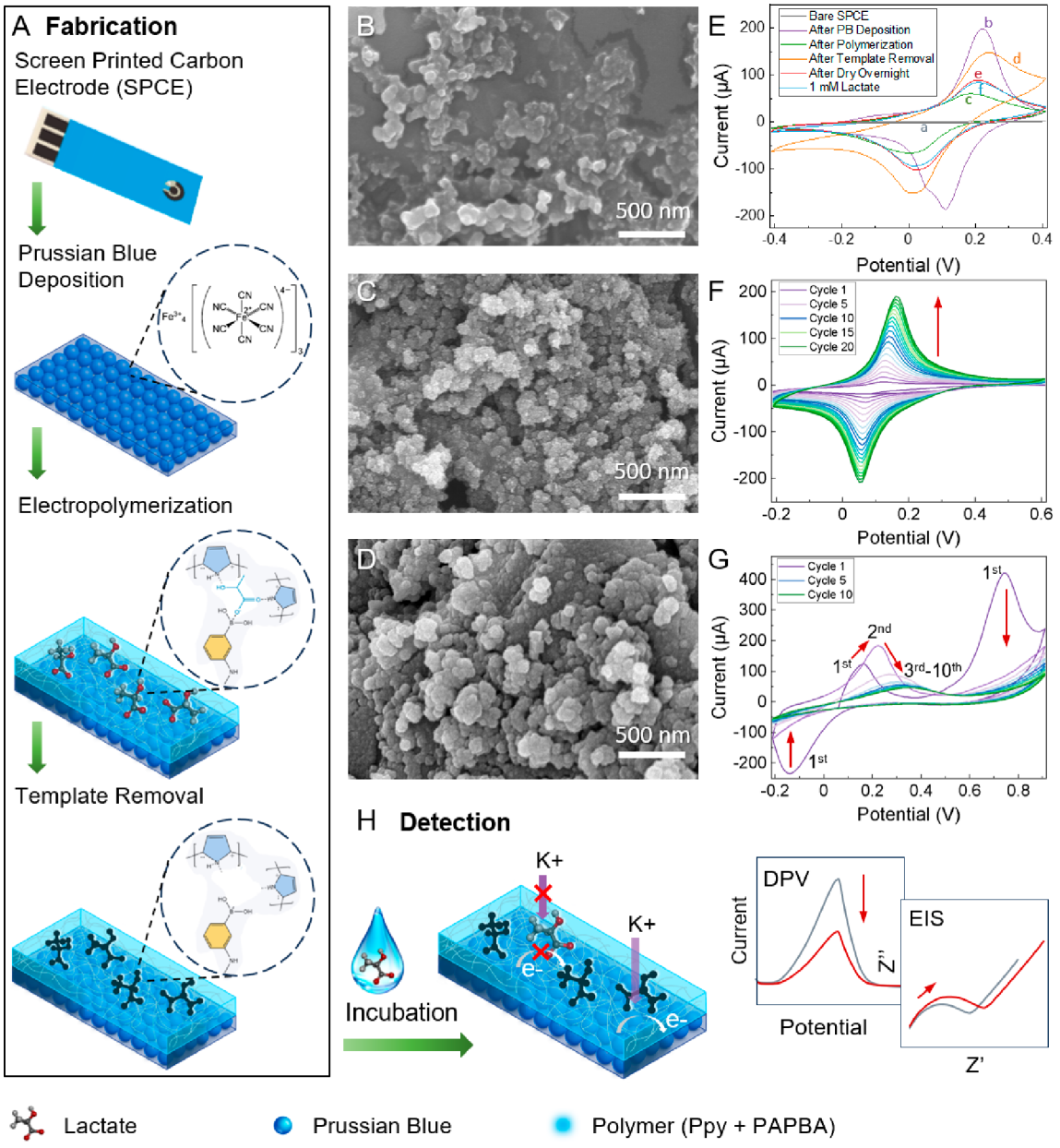

Figure 1. (A) The schematic of the fabrication process of eMIP/PB/SPCE-based sensor; FE-SEM image of (B) the bare SPCE, (C) PB/SPCE, and (D) eMIP/PB/SPCE; (E) characteristic CV curves measured in 0.1 M KCl for (a) the bare SPCE, (b) after PB deposition (PB/SPCE), (c) after eMIP polymerization, (d) after lactate template removal, (e) eMIP/PB/SPCE next day after drying overnight, and (f) after 1 mM lactate incubation; cyclic voltammograms of (F) PB electrodeposition and (G) electropolymerization of 50 mM 3-APBA, 100 mM pyrrole, and 10 mM lactate on PB/SPCE, and (H) an illustration of lactate detection mechanism showing the partially filled eMIP blocking electron transfer and the corresponding DPV and EIS responses.

containing pyrrole and 3-APBA in various concentrations and ratios, along with 10 mM lactate in 0.1 M KCl and 10 mM PBS (pH 7.4). Electropolymerization was carried out using CV, cycling from −0.2 to 0.9 V at 50 mV s^{-1} for a certain number of cycles. Upon completion of the electropolymerization, the electrode, denoted as eMIP/PB/SPCE, was immediately rinsed with water to eliminate any excess monomer. Subsequently, 160 μL of an 8% acetic acid solution was added to the electrode for template elution for 2 h. After the template removal, the electrodes were rinsed thoroughly with water and left to air-dry overnight.

2.5. Electrochemical Characterization and Performance Evaluation. The electrochemical characterization of the eMIP/PB/SPCE-based sensor was conducted in a 0.1 M KCl (pH 6.5) solution, which simulates the pH of sweat, and sensor performance was evaluated in both 0.1 M KCl solution and an artificial sweat (AS, pH 6.5) containing 85 mM NaCl, 15 mM KCl and 15 mM urea.[33] CV was used to characterize the sensor after each fabrication step. DPV was performed between −0.4 and 0.4 V to detect lactate under the following conditions: pulse amplitude: 50 mV; pulse width: 50 ms; pulse time: 0.05 s; scan rate: 10 mV s^{-1}. EIS was measured from 1 Hz to 100,000 Hz with a direct current (DC) bias of 0.16 V and alternating current (AC) amplitude of 0.02 V. For the detection process, a 100 μL volume of a blank solution (0.1 M KCl or AS, pH 6.5) was applied to the sensor and incubated for 10 min to eliminate potential baseline drift. The initial CV (5 cycles) and DPV or EIS (taken in triplicate) were recorded for the 0 mM concentration. Then, the sample bubble was spiked with a lactate stock solution (100 mM lactate in 0.1 M KCl, pH 6.5) to incrementally attain a total concentration ranging from 1 mM to 35 mM in the sample bubble. This was achieved by adding appropriate volumes of the stock

https://doi.org/10.1021/acsami.3c19448
ACS Appl. Mater. Interfaces 2024, 16, 66921−66931

solution to the sample bubble sequentially. After a 10 min incubation period in each spiked lactate concentration, triplicate DPV or EIS measurements were recorded. An EIS time scan was also carried out from 10 to 1000 Hz over a period of 1200 s to investigate the real-time impedance response to lactate binding. In this process, the solution bubble was spiked every 4 min with incremental volumes of lactate stock solution, and EIS was continuously recorded with an interval of 35 s for each frequency scan.

2.6. EC-SPR Characterization and Validation. For a more comprehensive understanding of the electropolymerization and rebinding process, the entire fabrication and detection procedure was carried out on a gold chip by using a surface plasmon resonance (SPR) spectrometer in conjunction with an electrochemical flow cell and a potentiostat. The experimental setup is discussed in more detail in section 3.4.

3. RESULTS AND DISCUSSION

3.1. Morphological and Electrochemical Characterization of eMIP/PB/SPCE. The fabrication process and detection mechanism of eMIP/PB/SPCE are depicted in Figure 1A and 1H, and the surface morphologies and electrochemical characteristics of the electrode after each fabrication step are presented in Figure 1B–G. The cleaned bare SPCE shows a rough surface (Figure 1B) and no redox activity in 0.1 M KCl (Figure 1E, curve a). PB nanoparticles were first electrodeposited on the SPCE working electrode using CV. This process involves the reduction of $Fe^{III}(CN)_6^{3-}$ to $Fe^{II}(CN)_6^{4-}$, resulting in the formation of $Fe_4^{III}[Fe^{II}(CN)_6]_3$ with Fe^{3+} in the solution.[34] The cyclic voltammograms recorded during the electrodeposition of PB (Figure 1F) exhibit a pair of cathodic and anodic peaks, initially located at 0.07 and 0.12 V, respectively, and gradually shifted to 0.06 and 0.16 V by the 20th cycle. The peak current gradually increased after each potential sweep cycle, indicating the steady formation of PB. The deposited PB nanoparticles covered the electrode surface, increasing the surface area of the working electrode (Figure 1C) and introducing notably high redox activity to the electrode in 0.1 M KCl (Figure 1E, curve b).

Following PB deposition, the electropolymerization of pyrrole and 3-APBA was conducted in the presence of lactate to create a polymer film with embedded lactate molecules. As shown in Figure 1G, the initial cycles (1st and 2nd) of electropolymerization reveal a redox couple around 0.2 and −0.15 V, which corresponds to the oxidation/reduction of the PB layer. A distinctive high current peak around 0.7 V and a pronounced tail at 0.9 V were observed, showing the characteristics of 3-APBA and pyrrole electropolymerization, respectively. An in-depth discussion of the characteristics of electropolymerization can be found in the Supporting Information (Supplemental Notes 1). As the polymerization progresses, the PB layer is covered by the polymer film, leading to diminished peaks of PB oxidation/reduction due to the insulating nature of the polymer film. The overall current decreases as the number of polymerization cycles increases. The SEM image of the electrode after eMIP deposition, presented in Figure 1D, exhibits cauliflower-like features of the polymer, which encapsulates PB nanoparticles on the PB/SPCE electrode surface. After electropolymerization, the redox activity of the electrode was greatly suppressed, as demonstrated in Figure 1E, curve c, which is attributable to the electron transfer and K^+ exchange being blocked by the polymer layer. After template elution in 8% acetic acid, lactate molecules are extracted from the polymer matrix, forming lactate cavities and leading to an increased redox activity, as shown in Figure 1E, curve d. This can be ascribed to the partially restored electron transfer ability and K^+ pathway with the created cavities.

Upon completion of the fabrication process, the eMIP/PB/SPCE-based sensor was left to dry overnight, during which a decrease in the redox current was observed (Figure 1E, curve e). When adding 1 mM lactate to the sensor, a slight decrease in PB oxidation/reduction peaks was observed (Figure 1E, curve f), indicating the rebinding of lactate molecules to the polymer matrix and the subsequent hindrance of the electrochemical activity, as depicted in Figure 1H. Given the relatively low sensitivity of CV, which carries background charging current, DPV and EIS are employed for lactate detection.[23]

3.2. PB Optimization and Stability. The number of PB nanoparticles is essential for achieving optimal sensor sensitivity. It should be sufficient to provide adequate redox current as an internal signal probe but not in excess to hinder complete encapsulation by an eMIP layer. Multiple rounds of PB deposition (20 CV cycles for each round) were conducted, each followed by eMIP layer electropolymerization, and the resulting sensing performance was evaluated. As shown in Figure S1A, the redox current during PB deposition by CV progressively increases within the same round and leaps to a higher level in the subsequent round with a fresh deposition solution when more reactants are introduced. As a result, the increased PB layer thickness enhances the redox signal. However, an optimized eMIP layer atop three rounds of PB deposition presents a high redox signal but low responses to lactate (Figure S1B). This can be attributed to the incomplete coverage of the thick PB layer by the eMIP layer, leading to unobstructed electron and K^+ pathways that remain unresponsive to changes in the lactate concentration. Therefore, the PB deposition was limited to a single round of 20 CV cycles, which provides a balance between signal intensity and response to lactate. The stability of the deposited PB nanoparticles (one round) was confirmed by cycling the PB/SPCE electrode in 0.1 M KCl solution for 100 cycles, demonstrating excellent signal stability (Figure S2A). As K^+ plays an important role in the PB signal, the impact of the K^+ concentration in the electrolyte was investigated by performing CVs on PB/SPCE in 0.1 M KCl and 2 KCl. As shown in Figure S2B, increasing the KCl concentration in the electrolyte shifts the redox potentials of PB but does not modulate the oxidation peak current. This suggests that changes in K^+ concentration in the electrolyte are unlikely to affect the sensor response, which is based on the oxidation peak current. While the absence of K^+ could potentially impact sensor sensitivity, this is unlikely to occur given that sweat always contains K^+.

3.3. Optimization of eMIP Electropolymerization. Electropolymerization parameters determine eMIPs' performance. In this study, two key factors were optimized: polymer concentration and the number of polymerization cycles. These parameters, identified previously by our research group during the development of cortisol-eMIP sensors, have a significant impact on eMIP performance.[35] Given the extensive design space, optimization of fabrication parameters was carried out through iterative random sampling using the univariate method in the following sequence: number of polymerization cycles and monomer ratios followed by cross-validation of the number of polymer cycles with the optimal monomer ratio.

https://doi.org/10.1021/acsami.3c19448
ACS Appl. Mater. Interfaces 2024, 16, 66921−66931

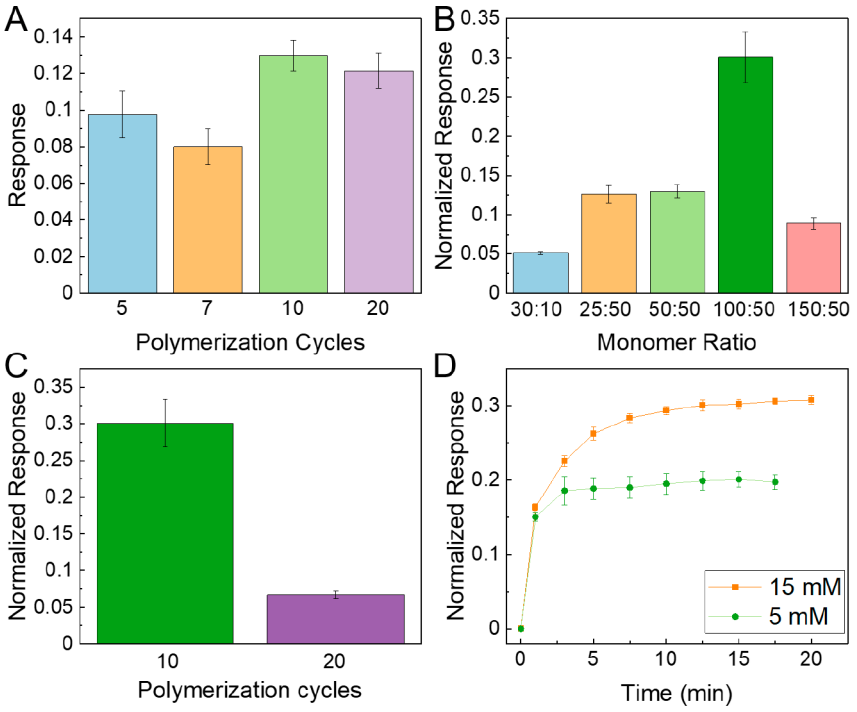

Figure 2. eMIP Optimization. Normalized DPV responses of sensors fabricated with (A) polymerization cycles of 5, 7, 10, and 20 in a solution of 50 mM:50 mM pyrrole and 3-APBA, (B) polymerization cycles of 10 in a solution containing monomer concentrations of 30:30, 25:50, 50:50, 100:50, and 150:50 mM (pyrrole: 3-APBA), (C) polymerization cycles of 10 and 20 in a solution of 100 mM pyrrole and 50 mM 3-APBA, and (D) normalized DPV responses of the optimized sensor over time while incubating in 5 and 15 mM lactate solution. Error bars are expressed as sample standard deviations (n = 4).

The number of polymerization cycles was first examined by using a polymerization solution of 50 mM 3-APBA and 50 mM pyrrole (a 1:1 ratio, totaling 100 mM monomers). The sensing performance of the eMIP/PB/SPCE made with polymerization cycles of 5, 7, 10, and 20 cycles was assessed. As shown in Figure 2A, sensors fabricated with ten polymerization cycles outperformed those made with other cycle numbers when evaluating the normalized current response. It is defined as the difference between the DPV peak currents in the blank (0 mM) and 15 mM lactate solution, normalized to the DPV peak current of the sensor in the blank solution (as per eq 1).

$$\text{response} = \frac{i_{\text{blank}} - i_{\text{15mM}}}{i_{\text{blank}}} \quad (1)$$

Normalizing the response is crucial for evaluating sensors fabricated with different parameters and accounting for sensor baseline variability. Repeating sensor recipes across various electrodes often shows slightly different blank peak currents due to inherent variability among these commercially purchased electrodes.

Upon identifying the preliminary optimal number of polymerization cycles, different monomer concentrations/ratios were tested, keeping the polymerization cycle number constant at 10. Sensors fabricated with various monomer concentrations/rations were examined, including 30:10, 25:50, 50:50, 100:50, and 150:50 (pyrrole:3-APBA, in mM). It is important to note that the maximum achievable concentration of 3-APBA is 50 mM. Beyond that, 3-APBA would not fully dissolve in the PBS KCl solution, resulting in an unknown saturation concentration of dissolved 3-APBA and excess 3-APBA particulates in the solution. This experiment revealed that the highest normalized response was achieved with a concentration of 100 mM pyrrole and 50 mM 3-APBA, as shown in Figure 2B. Since the sensor fabricated with 20 polymerization cycles showed a very close response to those fabricated with 10 cycles when testing the original monomer concentrations (Figure 2A), the newly optimized recipe was cross-referenced with 20 polymerization cycles to confirm the local optimum. As depicted in Figure 2C, the sensor with 20 polymerization cycles of 100 mM pyrrole and 50 mM 3-APBA showed a significantly reduced sensitivity, possibly due to the increased thickness of the polymer on the electrode surface.[36] A thick polymer layer can cause lactate molecules to become deeply embedded within the eMIP matrix, making them difficult to remove during template elution. It can also decrease PB activity due to the insulating nature of the polymer layer and blocked ion transfer. The same phenomenon was also observed in sensors fabricated with higher monomer concentrations.

On the contrary, when the number of polymerization cycles and monomer concentrations are too low, a decline in electrode sensitivity is observed. A thin eMIP layer often lacks a sufficient number of cavities, leading to inadequate molecular recognition.

The response kinetics of the optimized eMIP/PB/SPCE was assessed, as displayed in Figure 2D. This was achieved by measuring the DPV responses over a period of 20 min at an interval of 2.5 min while the sensor was incubated with 5 and 15 mM lactate. The sensor reached a plateau after 3 min of incubation with 5 mM lactate and after 10 min of incubation with 15 mM lactate. The increased response time observed with increasing lactate concentration highlights the necessity of allowing for interaction time to facilitate the diffusion and

https://doi.org/10.1021/acsami.3c19448
ACS Appl. Mater. Interfaces 2024, 16, 66921−66931

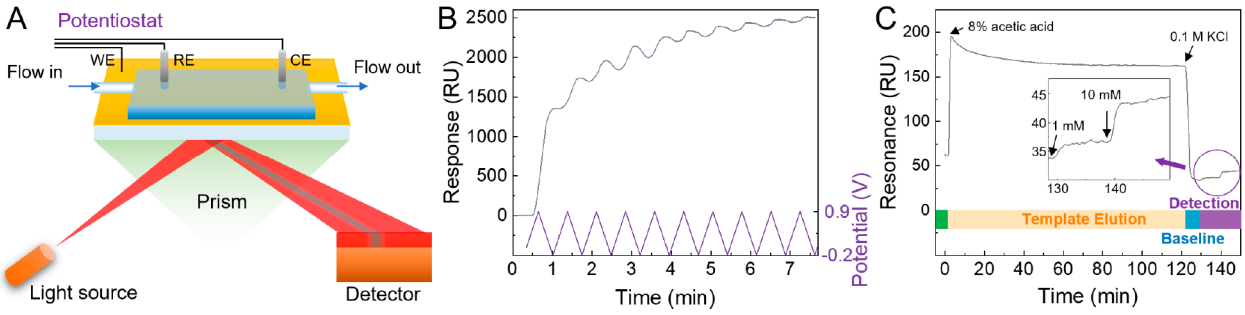

Figure 3. Surface plasmon resonance validation study. (A) Schematic of the EC-SPR spectrometer, (B) SPR sensorgram during electropolymerization where the cycling potential can be seen in comparison to the SPR response data, and (C) SPR sensorgram of eMIP/Au slide after electropolymerization (green) followed by template elution (orange), baseline in 0.1 M KCl (blue), and incubation with 1 and 10 mM lactate (purple).

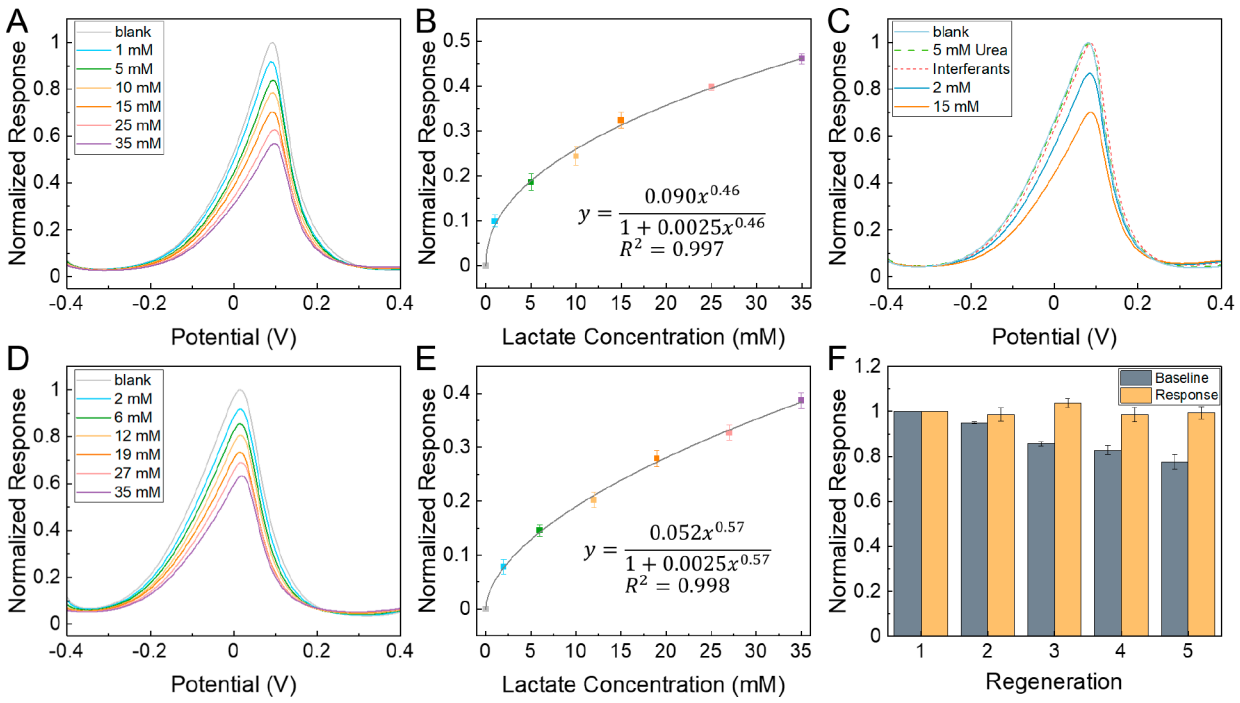

Figure 4. Lactate DPV detection. (A) Normalized DPV response to various lactate concentrations in 0.1 M KCl and (B) corresponding calibration curve. (C) Normalized DPV response in 0.1 M KCl solution with sequential additions of 5 mM urea, a mixture of interferants containing 50 μM glucose, 50 μM acetaminophen, 50 μM ascorbic acid, and 50 μM uric acid, 2 mM lactate, and 13 mM lactate (totaling 15 mM lactate). (D) Normalized DPV response to various lactate concentrations in artificial sweat and (E) corresponding calibration curve, error bars are expressed as the sample standard deviation (n = 4). (F) Normalized DPV baseline (baselines in 0.1 M KCl after each regeneration normalized to the original baseline before regeneration) and performance (response to 15 mM normalized to new baseline after each regeneration) averaged across 3 different electrodes and 5 regenerations. Error bars are expressed as sample standard deviation (n = 3).

binding of the analyte to eMIP. Therefore, an incubation time of 10 min was chosen for all tests.

3.4. Electrochemical-Surface Plasmon Resonance (EC-SPR) Study. To gain a comprehensive understanding of the electropolymerization process and validate the template removal and rebinding between lactate molecules and eMIP, EC-SPR analysis was performed. The SPR response was recorded while electropolymerization took place on a gold chip, which was conducted in a static cell containing the polymerization solution with the optimized recipe. As illustrated in Figure 3A, a gold chip, serving as the working electrode, was positioned on a glass prism, and covered with an electrochemical flow cell. The cell contained a platinum wire and a silver wire, functioning as the counter and pseudoreference electrode, respectively. A gold wire, affixed to the gold chip surface, extends outside of the flow cell for a potentiostat connection. The flow cell was equipped with an inlet and an outlet for introducing various solutions with a peristaltic pump to control the flow. This setup enabled simultaneous SPR measurement while performing electrochemical experiments such as electropolymerization. As shown in Figure 3B, the first cycle of electropolymerization resulted in the most substantial deposition on the surface, as indicated by the remarkable increase in resonance. Throughout the polymerization process, each cycle contributed to an incremental resonance rise, resembling a staircase. Most of this growth occurs in the voltage range between 0.4 and 0.9 V. Resonance drop was observed during the cathodic sweep toward −0.2 V in each cycle, possibly attributable to the repulsion of negatively charged ions. The net resonance increases after each CV cycle

https://doi.org/10.1021/acsami.3c19448
ACS Appl. Mater. Interfaces 2024, 16, 66921−66931

Table 1. Lactate Sensors with Biological Applications[a]

Matrix Tested	Sensing Mechanism	Concentration Range	LOD	Shelf Stability	Detection Method	Ref.
Breath	LOx	50−250 μM	465 nM	2 days at room temp, 1 week at 4 °C, 6 weeks at −20 °C	Electrochemical; Amperometric	41
Sweat	LOx/PB mediated	15 μM−30 mM	32.6 μM		Electrochemical	26
Sweat	LOx	1−50 mM			Electrochemical; Amperometric	42
Sweat	LOx/TMB	1 mM−30 mM	0.06 mM		Colorimetric	43
Sweat and Blood	LOx/PB mediated	1 mM−20 mM	0.12 mM	30 days at 4 °C	Electrochemical	11
Blood	LOx	1−40 mg/dL	0.053 mg/dL	3 days	Optical	15
PBS	MIP	0.1−1.7 mM	0.162 mM	2 weeks at 4 °C	UV−vis	44
Sweat	LOx	1 mM−24 mM			Electrochemical; Amperometric	28
Artificial Sweat	MIP	1 mM−20 mM			Electrochemical; DPV	45
Sweat	MIP/AgNW/Redox	1 μM−100 mM	0.22 μM	7 months in dark at room temp	Electrochemical; DPV	12
Sweat	MIP(PANI-*co*-3-APBA)/AuNP	4.5 mM−56 mM	2.2 mM	14 days at 4 °C	Electrochemical; DPV	46
Sweat	TTF/LOx	1 mM−20 mM		5 months at 4 °C	Electrochemical; Amperometric	3
Artificial Sweat	eMIP/PB/SPCE	1 mM−35 mM	0.20 mM	10 months at room temp	Electrochemical; DPV	This work

[a]AgNW: Silver nanowires. AuNP: Gold nanoparticles. LOx: Lactate oxidase. PANI: Polyaniline. TTF: Tetrathiafulvalene. TMB: 3,3′,5,5′-tetramethylbenzidine.

and gradually decreases as polymerization proceeds, which can be ascribed to the self-limiting electropolymerization due to the increased insulation of the growing film and possible depletion of monomers within the system.

Following the electropolymerization of the eMIP on the Au slide, the template removal step of incubation in 8% acetic acid for 2 h was performed with the flow cell at a constant flow rate of 40 μL min^{-1}. The introduction of 8% acetic acid changes the reflective index, leading to an upshift of the baseline. As shown in Figure 3C, the resonance gradually decreased in 8% acetic acid, indicating the removal of lactate and any excess monomers. After 2 h of elution, 0.1 M KCl solution was introduced to the flow cell to obtain a stable baseline. Subsequently, 1 mM lactate in 0.1 M KCl was flowed into the cell, leading to an initial rapid increase in resonance that gradually slowed down, signifying typical MIP absorption kinetics.[37] After introducing 10 mM lactate in 0.1 M KCl to the cell, a much higher increase in resonance was observed, showcasing the increased binding between lactate and eMIP/Au.

3.5. Detection of Lactate. Lactate detection was first carried out in 0.1 M KCl (pH 6.5) solution using DPV. The detection performance of the optimized eMIP/PB/SPCE is illustrated in Figure 4. With increasing lactate concentration, the DPV peak currents decrease, as shown in Figure 4A. This is attributed to the binding of lactate to the eMIP layer, which impedes the transfer of K^+ through the eMIP and the associated electron transfer of PB (Figure 1H). The PB/SPCE was also tested for lactate detection and was found to be nonresponsive, as shown in Figure S5.

The calibration curve is shown in Figure 4B. The reduction in the DPV peak current with increasing lactate concentrations can be accurately described using the Langmuir−Freundlich (L-FI) absorption isotherm model. Ghadeer et al. provided insights into the characterization of different absorption models for MIP films used in molecular detection.[38] It was noted that the L-FI model is suitable for systems featuring both heterogeneous and homogeneous binding sites at low, high, and saturation concentrations.[38] The Langmuir isotherm (L) typically models homogeneous systems, while the Freundlich isotherm (FI) addresses heterogeneous systems. The hybrid L-FI model successfully captures both types of systems,[39] and it can be expressed using eq 2.

$$B = \frac{N_t a C_e^m}{1 + a C_e^m} \tag{2}$$

where B is the concentration of bound analyte, C_e is the free analyte concentration, m is the heterogeneity index, N_t is the total number of binding sites, and a is related to the affinity constant, $K_0 = a^{1/m}$. The calibration had a high correlation factor (R^2) of 0.997. The limit of detection (LOD) and limit of quantification (LOQ) were 0.20 mM and 0.68 mM, calculated as the lactate concentration corresponding to a signal-to-noise ratio of 3 and 10 for the DPV measurements, respectively.

3.6. Detection of Lactate in Artificial Sweat. Lactate detection was also performed in artificial sweat (pH 6.5), as shown in Figure 4D, with the corresponding calibration curve presented in Figure 4E. The responses in the artificial sweat were slightly suppressed compared to the 0.1 M KCl solution (pH 6.5). The LOD and LOQ were determined to be 0.62 and 2.61 mM, respectively, which are slightly higher than those obtained in the KCl solution testing. In the literature, the relevant range of lactate detection is up to 25 or 30 mM for sporting applications.[40] Our developed here successfully covers this range in artificial sweat.

3.7. Selectivity of eMIP/PB/SPCE Sensor. One of the key advantages of MIP-based electrochemical sensors is their selective recognition, achieved through the formation of analyte cavities during the imprinting process. The selectivity of the eMIP/PB/SPCE-based sensors was evaluated by assessing their responses to various potential interferants, including 5 mM urea, 50 μM glucose, 50 μM acetaminophen, 50 μM ascorbic acid, and 50 μM uric acid. No significant distinction was observed in the DPV responses of the blank

https://doi.org/10.1021/acsami.3c19448
ACS Appl. Mater. Interfaces 2024, 16, 66921−66931

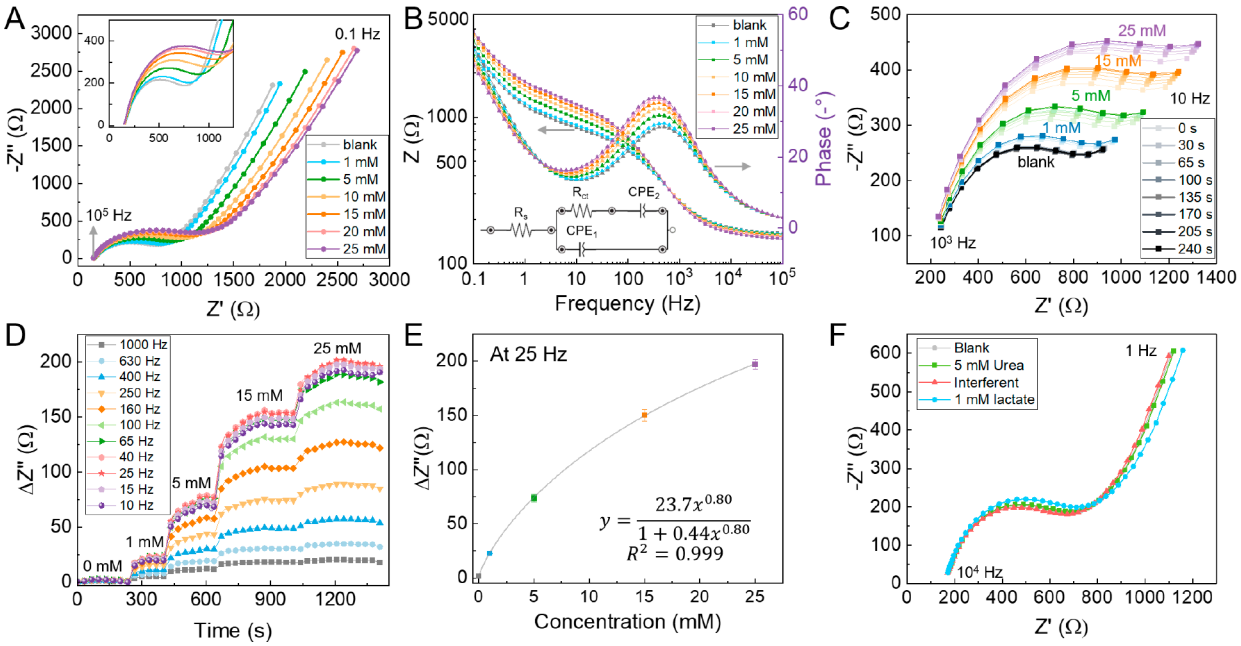

Figure 5. EIS Detection. (A) EIS Nyquist plot (insert: enlarged plot at the high-frequency range) and (B) Bode plot (insert: equivalent circuit), (▲) phase and (■) impedance of blank 0.1 M KCl, 1 mM, 5 mM, 10 mM, 15 mM, 20 mM, and 25 mM lactate. (C) Continuous EIS scan over time from 10 to 1000 Hz with 35 s intervals for blank 0.1 M KCl, 1 mM, 5 mM, 15 mM, and 25 mM lactate. (D) Imaginary impedance change versus time at frequencies between 10 and 1000 Hz. (E) Calibration curve of imaginary impedance change measured at 25 Hz, and (F) EIS of blank 0.1 M KCl solution with sequential additions of 5 mM glucose, 50 μM acetaminophen, 50 μM ascorbic acid, and 50 μM uric acid, and 1 mM lactate. Error bars are expressed as sample standard deviation (n = 3).

solution and after incubating with interferents for 10 min, as shown in Figure 4C.

Following incubation with the interferents, lactate incubation was conducted at concentrations of 2 and 15 mM. The responses align with the detection performed in 0.1 M KCl solution, indicating that the sensors remain sensitive to lactate even when coincubated with the interfering molecules. Thus, the sensor demonstrated excellent selectivity against all tested interferents and maintained its sensitivity to lactate.

3.8. Stability and Regeneration of the eMIP/PB/SPCE Sensor. The sensors also exhibit excellent shelf life and response stability, as illustrated in Figure 4F (Figure S6 presents the raw data and normalized responses after each regeneration). Three electrodes were continuously regenerated using 8% acetic acid over five repetitions. After each regeneration, the DPV peak current in the blank 0.1 M KCl was recorded and normalized against the original peak current and calculated using eq 3.

$$\text{baseline} = \frac{i_{\text{regeneration,0mM}}}{i_{\text{original,0mM}}} \quad (3)$$

The regenerated baseline exhibits a gradual downward drift over time, with approximately a 20% reduction after 5 repetitions. However, when assessing the sensor's performance using normalized response calculated with eq 1, the sensor response remains relatively consistent across the 5 trials. This indicates the sensors' ability to be reused for lactate detection using normalized responses without the need for recalibration. While there may ultimately be a limit to the reusability of the electrodes due to the drifting signals, these results demonstrate significant promise for the development of reusable sensors for lactate detection.

Furthermore, the tested sensors exhibited shelf stability and continued to provide responses even after being stored for 10 months under ambient conditions, as evidenced by the sensing data shown in Figure S7, tested in 0.1 M KCl. The sensors developed herein exhibited a stability far greater than other enzymatic lactate sensors from the literature, as shown in Table 1. When compared to other MIP-based lactate sensors, the eMIP/PB/SPCE sensor developed in this study offers a comparable LOD and covers the full application range of lactate concentrations, all successfully through a reagent-free detection process.

3.9. Electrochemical Impedance Spectroscopy Study. The performance of the optimized sensors was also evaluated by using electrochemical impedance spectroscopy (EIS). The impedance spectra of the sensor were initially measured after 10 min of incubation in 0.1 M KCl (pH 6.5) and various lactate concentrations. Nyquist plots, which plot the real impedance (Z') against the imaginary impedance (Z''), are presented in Figure 5A. As lactate concentrations increase, the diameter of the semicircle in the EIS curves also increases, indicating increased electron transfer resistance. The proposed equivalent circuit model, shown in the inset of Figure 5B, provides a good fitting over the tested frequency range. This equivalent circuit is a modified version of the Randles circuit, comprising the electrolyte solution resistance (R_s), a constant phase element (CPE_1) representing the capacitance of the electric double layer formed at the interface of the eMIP/PB/SPCE biosensor and the electrolyte solution, and a parallel charge transfer resistance R_{ct}. Notably, the Nyquist plots exhibit a straight line at low frequencies, which is not 45 deg. This may be attributed to the influence of the electrode inhomogeneity. Therefore, a constant phase element (CPE_2) was included in series with R_{ct} instead of a traditional Warburg element for semi-infinite diffusion. A similar response was

https://doi.org/10.1021/acsami.3c19448
ACS Appl. Mater. Interfaces 2024, 16, 66921−66931

observed with a PB enzymatic sensor designed for the detection of urea.[47]

The same data set can also be presented in the Bode diagram, enabling the visualization of phase (▲) and impedance (■) changes over the frequency range. As shown in Figure 5B, with increasing lactate concentration, phase and impedance values showed the most significant changes in the frequency range of 10 to 1000 Hz. To probe the binding kinetics, this frequency range was used in a semi-real-time detection study, where impedance spectra were continuously measured from 10 to 1000 Hz at a 35 s interval, as depicted in Figure 5C. While the impedance spectra were recorded continuously, the detection solution was spiked with an increased concentration of lactate at a 4 min interval. The diameter of the impedance spectra immediately increased after each lactate concentration change and gradually reached an equilibrium. This continuous monitoring allowed for the real-time visualization of the sensor's response and stabilization at different lactate concentrations.

When extracting data from the initial test in Figure 5C, the response of different impedance parameters (i.e., Z, Z', Z'', and phase) at each tested frequency can be graphed over time. The imaginary impedance, Z'', provides the highest response to lactate concentration change at a fixed frequency compared to other parameters. As shown in Figure 5D, Z'' at some frequencies exhibited higher responses than others, with 25 Hz displaying the most sensitive response to changes in lactate concentration. Each concentration reached an equilibrium state within 4 min, demonstrating a rapid response time and the feasibility of real-time sweat detection. The stabilized response of Z'' at the 25 Hz frequency is graphed in response to the changes in lactate concentration, conforming to the Langmuir−Freundlich absorption model, Figure 5E. The sensors were also tested with interfering analytes using EIS measurements (Figure 5F). The sensor EIS measurements, much like their DPV measurements, show no responses to 5 mM Urea, 50 μM glucose, 50 μM acetaminophen, 50 μM ascorbic acid, and 50 μM uric acid and are still responsive to 1 mM lactate in a cointerferent solution.

4. CONCLUSION

In summary, this work has successfully demonstrated the development and optimization of an eMIP-based electrochemical sensor, utilizing PB nanoparticles as the internal signal probe, for reagent-free lactate detection. The processes of electropolymerization, template elution, and analyte rebinding were investigated and validated using EC-SPR, providing valuable insights into the polymer growth rate and lactate binding kinetics. The performance of eMIP/PB/SPCE-based sensors was thoroughly evaluated using DPV and EIS, demonstrating excellent sensitivity and selectivity toward lactate against potential interferents in a mixed environment. Notably, the sensors exhibited superior stability and a shelf life of up to 10 months under ambient conditions, outperforming traditional lactate sensors constructed with lactate oxidase and MIPs, as reported in the existing literature. Moreover, with data normalization, these sensors also displayed excellent reproducibility across devices and could be regenerated for use without the need for recalibration. Nevertheless, the current regeneration method is not feasible for an on-body operation. New regeneration methods and further optimizations are needed to progress toward a continuous monitoring system for sweat lactate detection. This approach holds the potential for broader applications, which can be expanded for the development of reagent-free eMIP-based electrochemical sensors for other electro-inactive analytes.

■ ASSOCIATED CONTENT

Data Availability Statement

The data that supports this study are available from the corresponding author upon reasonable request.

Supporting Information

The Supporting Information is available free of charge at https://pubs.acs.org/doi/10.1021/acsami.3c19448.

Electropolymerization characteristics, figures for PB optimization, PB stability and sensitivity to different KCl concentrations, electropolymerization characteristics of different recipes, CV characteristics of eMIP/SPCE, eNIP/SPCE, eMIP/PB/SPCE, and eNIP/PB/SPCE, triplicate DPV responses of PB/SPCE and eMIP/PB/SPCE, the eMIP/PB/SPCE regeneration test, and eMIP/PB/SPCE tested 10 months after fabrication (PDF)

■ AUTHOR INFORMATION

Corresponding Author

Yixin Liu − *Department of Chemical Engineering, Michigan Technological University, Houghton, Michigan 49931, United States*; orcid.org/0000-0002-3758-3145; Email: yixinliu@mtu.edu

Authors

Grace Dykstra − *Department of Chemical Engineering, Michigan Technological University, Houghton, Michigan 49931, United States*

Isabel Chapa − *Department of Chemical Engineering, Michigan Technological University, Houghton, Michigan 49931, United States*

Complete contact information is available at: https://pubs.acs.org/10.1021/acsami.3c19448

Notes

The authors declare no competing financial interest.

■ ACKNOWLEDGMENTS

We greatly appreciate the funding support from Michigan Technological University and the National Science Foundation (Award: 2138523).

■ REFERENCES

(1) Baker, L. B.; Wolfe, A. S. Physiological Mechanisms Determining Eccrine Sweat Composition. *Eur. J. Appl. Physiol* **2020**, *120* (4), 719−752.

(2) Chien, M.-N.; Fan, S.-H.; Huang, C.-H.; Wu, C.-C.; Huang, J.-T. Continuous Lactate Monitoring System Based on Percutaneous Microneedle Array. *Sensors* **2022**, *22* (4), 1468.

(3) Jia, W.; Bandodkar, A. J.; Valdés-Ramírez, G.; Windmiller, J. R.; Yang, Z.; Ramírez, J.; Chan, G.; Wang, J. Electrochemical Tattoo Biosensors for Real-Time Noninvasive Lactate Monitoring in Human Perspiration. *Anal. Chem.* **2013**, *85* (14), 6553−6560.

(4) Green, J. M.; Pritchett, R. C.; Crews, T. R.; McLester, J. R.; Tucker, D. C. Sweat Lactate Response between Males with High and Low Aerobic Fitness. *Eur. J. Appl. Physiol* **2004**, *91* (1), 1−6.

(5) Derbyshire, P. J.; Barr, H.; Davis, F.; Higson, S. P. J. Lactate in Human Sweat: A Critical Review of Research to the Present Day. *Journal of Physiological Sciences* **2012**, *62* (6), 429−440.

(6) Garland, N. T.; Schmieder, J.; Johnson, Z. T.; Hjort, R. G.; Chen, B.; Andersen, C.; Sanborn, D.; Kjeldgaard, G.; Pola, C. C.; Li, J.; Gomes, C.; Smith, E. A.; Angus, H.; Meyer, J.; Claussen, J. C. Wearable Flexible Perspiration Biosensors Using Laser-Induced Graphene and Polymeric Tape Microfluidics. *ACS Appl. Mater. Interfaces* **2023**, *15* (32), 38201−38213.
(7) Bandodkar, A. J.; Gutruf, P.; Choi, J.; Lee, K.; Sekine, Y.; Reeder, J. T.; Jeang, W. J.; Aranyosi, A. J.; Lee, S. P.; Model, J. B.; Ghaffari, R.; Su, C.-J.; Leshock, J. P.; Ray, T.; Verrillo, A.; Thomas, K.; Krishnamurthi, V.; Han, S.; Kim, J.; Krishnan, S.; Hang, T.; Rogers, J. A. Battery-Free, Skin-Interfaced Microfluidic/Electronic Systems for Simultaneous Electrochemical, Colorimetric, and Volumetric Analysis of Sweat. *Sci. Adv.* **2019**, *5* (1), No. eaav3294.
(8) Gao, W.; Emaminejad, S.; Nyein, H. Y. Y.; Challa, S.; Chen, K.; Peck, A.; Fahad, H. M.; Ota, H.; Shiraki, H.; Kiriya, D.; Lien, D.-H.; Brooks, G. A.; Davis, R. W.; Javey, A. Fully Integrated Wearable Sensor Arrays for Multiplexed in Situ Perspiration Analysis. *Nature* **2016**, *529* (7587), 509−514.
(9) Li, M.; Wang, L.; Liu, R.; Li, J.; Zhang, Q.; Shi, G.; Li, Y.; Hou, C.; Wang, H. A Highly Integrated Sensing Paper for Wearable Electrochemical Sweat Analysis. *Biosens Bioelectron* **2021**, *174*, No. 112828.
(10) Hojaiji, H.; Zhao, Y.; Gong, M. C.; Mallajosyula, M.; Tan, J.; Lin, H.; Hojaiji, A. M.; Lin, S.; Milla, C.; Madni, A. M.; Emaminejad, S. An Autonomous Wearable System for Diurnal Sweat Biomarker Data Acquisition. *Lab Chip* **2020**, *20* (24), 4582−4591.
(11) Xuan, X.; Chen, C.; Molinero-Fernandez, A.; Ekelund, E.; Cardinale, D.; Swarén, M.; Wedholm, L.; Cuartero, M.; Crespo, G. A. Fully Integrated Wearable Device for Continuous Sweat Lactate Monitoring in Sports. *ACS Sens* **2023**, *8* (6), 2401−2409.
(12) Zhang, Q.; Jiang, D.; Xu, C.; Ge, Y.; Liu, X.; Wei, Q.; Huang, L.; Ren, X.; Wang, C.; Wang, Y. Wearable Electrochemical Biosensor Based on Molecularly Imprinted Ag Nanowires for Noninvasive Monitoring Lactate in Human Sweat. *Sens Actuators B Chem.* **2020**, *320*, No. 128325.
(13) Kumar, N.; Lin, Y.-J.; Huang, Y.-C.; Liao, Y.-T.; Lin, S.-P. Detection of Lactate in Human Sweat via Surface-Modified, Screen-Printed Carbon Electrodes. *Talanta* **2023**, *265*, No. 124888.
(14) Shapiro, F.; Silanikove, N. Rapid and Accurate Determination of D- and l-Lactate, Lactose and Galactose by Enzymatic Reactions Coupled to Formation of a Fluorochromophore: Applications in Food Quality Control. *Food Chem.* **2010**, *119* (2), 829−833.
(15) Biswas, A.; Bornhoeft, L. R.; Banerjee, S.; You, Y.-H.; McShane, M. J. Composite Hydrogels Containing Bioactive Microreactors for Optical Enzymatic Lactate Sensing. *ACS Sens* **2017**, *2* (11), 1584−1588.
(16) Baretta, R.; Raucci, A.; Cinti, S.; Frasconi, M. Porous Hydrogel Scaffolds Integrating Prussian Blue Nanoparticles: A Versatile Strategy for Electrochemical (Bio)Sensing. *Sens Actuators B Chem.* **2023**, *376*, No. 132985.
(17) Crapnell, R.; Hudson, A.; Foster, C.; Eersels, K.; Grinsven, B.; Cleij, T.; Banks, C.; Peeters, M. Recent Advances in Electrosynthesized Molecularly Imprinted Polymer Sensing Platforms for Bioanalyte Detection. *Sensors* **2019**, *19* (5), 1204.
(18) Pirot, S. M.; Omer, K. M. Surface Imprinted Polymer on Dual Emitting MOF Functionalized with Blue Copper Nanoclusters and Yellow Carbon Dots as a Highly Specific Ratiometric Fluorescence Probe for Ascorbic Acid. *Microchemical Journal* **2022**, *182*, No. 107921.
(19) Yang, W.; Ma, Y.; Sun, H.; Huang, C.; Shen, X. Molecularly Imprinted Polymers Based Optical Fiber Sensors: A Review. *TrAC Trends in Analytical Chemistry* **2022**, *152*, No. 116608.
(20) Pirot, S. M.; Omer, K. M.; Alshatteri, A. H.; Ali, G. K.; Shatery, O. B. A. Dual-Template Molecularly Surface Imprinted Polymer on Fluorescent Metal-Organic Frameworks Functionalized with Carbon Dots for Ascorbic Acid and Uric Acid Detection. *Spectrochim Acta A Mol. Biomol Spectrosc* **2023**, *291*, No. 122340.
(21) Ali, G. K.; Omer, K. M. Molecular Imprinted Polymer Combined with Aptamer (MIP-Aptamer) as a Hybrid Dual Recognition Element for Bio(Chemical) Sensing Applications. Review. *Talanta* **2022**, *236*, No. 122878.
(22) Liu, Y.; Dykstra, G. Recent Progress on Electrochemical (Bio)Sensors Based on Aptamer-Molecularly Imprinted Polymer Dual Recognition. *Sensors and Actuators Reports* **2022**, *4*, No. 100112.
(23) Moreira Gonçalves, L. Electropolymerized Molecularly Imprinted Polymers: Perceptions Based on Recent Literature for Soon-to-Be World-Class Scientists. *Curr. Opin Electrochem* **2021**, *25*, 100640.
(24) Zidarič, T.; Majer, D.; Maver, T.; Finšgar, M.; Maver, U. The Development of an Electropolymerized, Molecularly Imprinted Polymer (MIP) Sensor for Insulin Determination Using Single-Drop Analysis. *Analyst* **2023**, *148* (5), 1102−1115.
(25) Dykstra, G.; Reynolds, B.; Smith, R.; Zhou, K.; Liu, Y. Electropolymerized Molecularly Imprinted Polymer Synthesis Guided by an Integrated Data-Driven Framework for Cortisol Detection. *ACS Appl. Mater. Interfaces* **2022**, *14* (22), 25972−25983.
(26) Xuan, X.; Pérez-Ràfols, C.; Chen, C.; Cuartero, M.; Crespo, G. A. Lactate Biosensing for Reliable On-Body Sweat Analysis. *ACS Sens* **2021**, *6* (7), 2763−2771.
(27) Matos-Peralta, Y.; Antuch, M. Review—Prussian Blue and Its Analogs as Appealing Materials for Electrochemical Sensing and Biosensing. *J. Electrochem. Soc.* **2020**, *167* (3), No. 037510.
(28) Payne, M. E.; Zamarayeva, A.; Pister, V. I.; Yamamoto, N. A. D.; Arias, A. C. Printed, Flexible Lactate Sensors: Design Considerations Before Performing On-Body Measurements. *Sci. Rep* **2019**, *9* (1), 13720.
(29) Karyakin, A. A. Prussian Blue and Its Analogues: Electrochemistry and Analytical Applications. *Electroanalysis* **2001**, *13*, 813.
(30) Tang, W.; Yin, L.; Sempionatto, J. R.; Moon, J.-M.; Teymourian, H.; Wang, J. Touch-Based Stressless Cortisol Sensing. *Advanced materials* **2021**, *33* (18), 2008465.
(31) Rattu, G.; Krishna, P. M. TiO2 Nanoparticles Reagent Based Nonenzymatic Label-Free Optical Sensor for the Rapid Detection of L-Lactate in Apple Juice. *Sensors and Actuators Reports* **2021**, *3*, No. 100067.
(32) Dhiraj, H. S.; Ishizuka, F.; Saeed, M.; Elshaer, A.; Zetterlund, P. B.; Aldabbagh, F. Lactate and Glucose Responsive Boronic Acid-Substituted Amphiphilic Block Copolymer Nanoparticles of High Aspect Ratio. *Eur. Polym. J.* **2023**, *185*, No. 111819.
(33) Tang, W.; Yin, L.; Sempionatto, J. R.; Moon, J.; Teymourian, H.; Wang, J. Touch-Based Stressless Cortisol Sensing. *Adv. Mater.* **2021**, *33* (18), 2008465.
(34) Karyakin, A. A. Prussian Blue and Its Analogues: Electrochemistry and Analytical Applications. *Electroanalysis* **2001**, *13* (10), 813−819.
(35) Dykstra, G.; Reynolds, B.; Smith, R.; Zhou, K.; Liu, Y. Electropolymerized Molecularly Imprinted Polymer Synthesis Guided by an Integrated Data-Driven Framework for Cortisol Detection. *ACS Appl. Mater. Interfaces* **2022**, *14* (22), 25972−25983.
(36) Tajik, S.; Beitollahi, H.; Nejad, F. G.; Shoaie, I. S.; Khalilzadeh, M. A.; Asl, M. S.; Van Le, Q.; Zhang, K.; Jang, H. W.; Shokouhimehr, M. Recent Developments in Conducting Polymers: Applications for Electrochemistry. *RSC Adv.* **2020**, *10* (62), 37834−37856.
(37) Gomes, J. C. M.; Souza, L. C.; Oliveira, L. C. SmartSPR Sensor: Machine Learning Approaches to Create Intelligent Surface Plasmon Based Sensors. *Biosens Bioelectron* **2021**, *172*, No. 112760.
(38) Abu-Alsoud, G. F.; Hawboldt, K. A.; Bottaro, C. S. Comparison of Four Adsorption Isotherm Models for Characterizing Molecular Recognition of Individual Phenolic Compounds in Porous Tailor-Made Molecularly Imprinted Polymer Films. *ACS Appl. Mater. Interfaces* **2020**, *12* (10), 11998−12009.
(39) Tamayo, F. G.; Casillas, J. L.; Martin-Esteban, A. Evaluation of New Selective Molecularly Imprinted Polymers Prepared by Precipitation Polymerisation for the Extraction of Phenylurea Herbicides. *J. Chromatogr A* **2005**, *1069* (2), 173−181.
(40) Payne, M. E.; Zamarayeva, A.; Pister, V. I.; Yamamoto, N. A. D.; Arias, A. C. Printed, Flexible Lactate Sensors: Design

https://doi.org/10.1021/acsami.3c19448
ACS Appl. Mater. Interfaces 2024, 16, 66921−66931

Considerations Before Performing On-Body Measurements. *Sci. Rep* **2019**, *9* (1), 13720.
(41) Zhang, S.; Chen, Y.-C.; Riezk, A.; Ming, D.; Tsvik, L.; Sützl, L.; Holmes, A.; O'Hare, D. Rapid Measurement of Lactate in the Exhaled Breath Condensate: Biosensor Optimization and In-Human Proof of Concept. *ACS Sens* **2022**, *7* (12), 3809−3816.
(42) Shitanda, I.; Ozone, Y.; Morishita, Y.; Matsui, H.; Loew, N.; Motosuke, M.; Mukaimoto, T.; Kobayashi, M.; Mitsuhara, T.; Sugita, Y.; Matsuo, K.; Yanagita, S.; Suzuki, T.; Mikawa, T.; Watanabe, H.; Itagaki, M. Air-Bubble-Insensitive Microfluidic Lactate Biosensor for Continuous Monitoring of Lactate in Sweat. *ACS Sens* **2023**, *8* (6), 2368−2374.
(43) Vaquer, A.; Barón, E.; de la Rica, R. Wearable Analytical Platform with Enzyme-Modulated Dynamic Range for the Simultaneous Colorimetric Detection of Sweat Volume and Sweat Biomarkers. *ACS Sens* **2021**, *6* (1), 130−136.
(44) Mustafa, Y. L.; Leese, H. S. Fabrication of a Lactate-Specific Molecularly Imprinted Polymer toward Disease Detection. *ACS Omega* **2023**, *8* (9), 8732−8742.
(45) Kanokpaka, P.; Chang, L.-Y.; Wang, B.-C.; Huang, T.-H.; Shih, M.-J.; Hung, W.-S.; Lai, J.-Y.; Ho, K.-C.; Yeh, M.-H. Self-Powered Molecular Imprinted Polymers-Based Triboelectric Sensor for Non-invasive Monitoring Lactate Levels in Human Sweat. *Nano Energy* **2022**, *100*, No. 107464.
(46) Mugo, S. M.; Robertson, S. V.; Lu, W. A Molecularly Imprinted Screen-Printed Carbon Electrode for Electrochemical Epinephrine, Lactate, and Cortisol Metabolites Detection in Human Sweat. *Anal. Chim. Acta* **2023**, *1278*, No. 341714.
(47) Valiuniene, A.; Kavaliauskaite, G.; Virbickas, P.; Ramanavicius, A. Prussian Blue Based Impedimetric Urea Biosensor. *J. Electroanal. Chem.* **2021**, *895*, No. 115473.

https://doi.org/10.1021/acsami.3c19448
ACS Appl. Mater. Interfaces 2024, 16, 66921−66931